Analysis of resonance structure in the above-threshold ionization photoelectron spectra of magnesium

G. D. Gillen* and L. D. Van Woerkom
Department of Physics, The Ohio State University, 174 West 18 Avenue, Columbus, Ohio 43210-1106, USA
(Received 22 April 2003; published 5 September 2003)

Using high-resolution photoelectron spectroscopy and 120-fs, 800-nm Ti:sapphire laser pulses, we observe and analyze intensity-dependent resonant population of specific intermediate excited states of neutral magnesium atoms and their subsequent photoionization in the laser field. Various participating states are identified using angular-momentum selection rules, partial yields, and angular distributions. Several unexpected results are observed and discussed, including peaks that do not correspond to expected resonant processes, and order-to-order variations in the photoelectron spectra.

DOI: 10.1103/PhysRevA.68.033401 PACS number(s): 42.50.Hz, 32.80.Rm

I. INTRODUCTION

Photoelectron spectra (PES) have been used quite extensively over the past 20 years as a tool to investigate what happens when matter is irradiated with high-intensity light. Multiphoton ionization (MPI) was first observed in 1965 by Voronov and Delone [1]. As peak laser intensities increased with the advancement of laser technology, the propensity for an atom to absorb more photons than the minimum required for ionization became non-negligible, and above-threshold ionization (ATI) was reported by Agostini *et al.* in 1979 [2]. In the earlier days the pulse widths of lasers were long with respect to the time taken by the ionized electron to leave the interaction region. PES for this long pulse regime yielded structureless peaks separated by a photon energy, revealing little information about the ionization dynamics other than the number of photons the electron absorbed and the relative probabilities for each order [3]. In 1987, Freeman *et al.* reported that as the laser pulse width decreased, the kinetic energy of each ATI order shifted to lower energy and broke apart into structured sub-peaks [3]. The peaks in the PES corresponded to population of specific atomic states during the ionization process and became known as Freeman resonances. The ability of shorter laser pulses to observe atomic transitions during the ionization process opened the door for a new field of study in high-intensity laser-atom interactions for peak laser intensities up to 10^{14} W/cm^2.

The majority of intense-field photoionization experiments in the intensity range of 10^{12}–10^{14} W/cm^2 have been performed using noble gases [3–5,7–11], and have yielded similar overall results. This intensity range is particularly interesting due to the prominence of Freeman resonances and the overall characteristics of such photoelectron spectra fall into four categories as follows: (1) The kinetic energies of the ejected electrons have a smooth, continuous background distribution. (2) On top of the continuous background are groups of ATI peaks separated by the photon energy with each having substructure. (3) The magnitudes of (1) and (2) first decrease exponentially for higher kinetic energies, and finally, (4) the distribution of kinetic energies has a ''plateau'' or extension beyond that of (3), where the detected photoelectron signal levels off, or decreases more slowly as a function of higher kinetic energies. All of these characteristics have been explained and theoretically modeled using single active electron and rescattering theories. Comparisons of experimental results and theory [12] indicate that for atoms with a closed outer shell the dominant process consists of only one electron interacting with the laser field at a time. Both the experiments and calculations for intermediate peak laser intensities (after application of a spatial and temporal probability weighted averaging algorithm) demonstrate the dominant role of resonant population and subsequent ionization of bound neutral states in the MPI and ATI of atoms.

In this paper we present high-resolution photoelectron spectra for magnesium atoms exposed to 800-nm, 120-fs laser pulses, with peak intensities of 10^{12}–10^{13} W/cm^2. The data reveal some of the expected behaviors of ATI PES for lower intensities, as well as some interesting peculiarities for higher intensities, which are not easily explained by traditional ATI models. The analysis and identification of various ATI peaks, as well as the unexpected variations of PES from previous experiments, will be presented and discussed.

II. EXPERIMENT

The laser system and general experimental setup used in this investigation is the same as that described previously [10]. The laser is focused into the vacuum chamber via a 250 mm focal length lens with an initial beam diameter of roughly 7 mm. The laser propagation direction, atomic beam path, and flight tube axis are all mutually orthogonal. The interaction region used to collect the data is located between a pinhole plate and the open end of the flight tube. Due to collimating apertures, the width of the atomic beam in this region is 2 mm. Using this focal geometry and 800-nm light, the Rayleigh range is about 1.5 cm. Even though the width of the interaction region exposed to the detector is larger than previous experiments [4–7,12], the condition that the interaction region exposed to the detector is smaller than the Rayleigh range is still satisfied in order for a restricted volume

*Present address: Air Force Research Laboratory, Anteon Corporation, Building 71A, Area B, Wright Patterson Air Force Base, OH 45433.

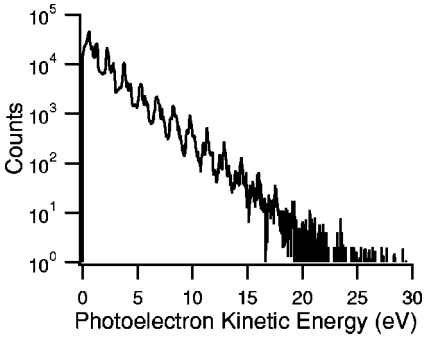

FIG. 1. Photoelectron spectra of magnesium atoms exposed to 33 TW/cm^2, 120-fs, 800-nm light pulses.

experiment to be considered. The flight path between the interaction region and the microchannel plates (MCPs) is 49.5 cm, and the flight tube is grounded and wrapped with multiple layers of high magnetic permeability μ-metal to ensure that the flight path of the electrons is free of any residual electrical or magnetic fields, enabling the detection of low-kinetic-energy electrons. Immediately prior to impacting the MCPs, the electrons are accelerated through an additional 900 V over a distance of 2 mm. The final accelerating potential reduces the difference in kinetic energy between a 1-eV electron and a 20-eV electron to only 2%, ensuring that the quantum efficiency of the MCPs is relatively constant over the kinetic-energy range of photoelectrons detected in this work.

The photoelectron spectra were collected by measuring the time difference between the laser pulse exiting the laser and the detection of each count by the MCPs. The time data were converted to kinetic energy and the signal normalized to 10^6 laser shots per spectrum. Up to 15×10^6 laser shots were taken per spectrum for lower intensities to obtain more accurate counting statistics.

III. RESULTS AND DISCUSSION

A. General PES characteristics

A sample PES for magnesium atoms exposed to a laser intensity of 33 TW/cm^2 is displayed in Fig. 1. Upon inspection, only three of the four characteristics discussed earlier for PES for the noble gases are present for magnesium: (1) The foundation of a smooth and continuous distribution of kinetic energy for the photoelectrons is evident from very low energies out to near 15 eV, where the signal begins to degrade into the noise level, (2) structured sets of peaks are arranged throughout the PES and separated by the energy of a single photon, 1.55 eV, and (3) there is a monotonic decrease in the signal as a function of higher-kinetic-energy. In this section we will first discuss the general characteristics of photoelectron spectra of magnesium: the monotonic decrease in signal and high kinetic energy cutoff. In Sec. III B we will discuss the structured peaks within the first few ATI orders, followed by an analysis of those peaks using partial yields (PYs) and angular distributions (ADs) in Sec. III C.

Results from both observed and calculated PES reveal that, for most elements, the number of counts or kinetic-energy probability for characteristic (3) should decrease monotonically from one order to the next. The exact rate and cutoff kinetic energy can depend upon a large number of different parameters, including the target element, laser frequency, peak intensity, dominant ionization mechanism, signal-to-noise ratio, etc. The effects of the first three of these on the ionization process are all somewhat intertwined. If the energy per photon is small compared to the binding energy of the ground state of the atom, and the distortion of the Coulomb potential due to the peak field is small with respect to the depth of the ground state, then multiphoton ionization is considered to be the dominant ionization mechanism. As the distortion of the Coulomb potential becomes non-negligible with respect to the depth of the ground state, and the tunneling time becomes comparable to the optical period, then tunneling ionization becomes the dominant mechanism. For experiments in the multiphoton or tunneling regimes it is convenient to discuss the combined effects of the laser frequency and the peak intensity by using the ponderomotive energy $U_p = I/(4\omega^2)$, in atomic units. The ponderomotive energy is simply the time-averaged kinetic energy of a free electron in an oscillating electric field with an intensity I and a frequency ω.

Depending upon the phase of the laser field at the time of ionization, the electron can escape from the core with a kinetic energy up to $2.5U_p$ [13], for a semiclassical tunneling ionization model. Lohr *et al.* also predicted the maximum kinetic energy for an electron ionized via multiphoton absorption, which appears in the continuum at the position of the core with some initial kinetic energy, to be $4.5U_p$ [13].

Once the electron is ionized, its motion is driven by the oscillating electric field of the laser under which it can collisionally reencounter the core. If an elastic-rescattering mechanism is a non-negligible process, then a cutoff of $10U_p$ is expected for the maximum kinetic energy of photoelectrons leaving the interaction region [13].

Thus, after the monotonic decrease in counts per ATI order, a much ''flatter'' region of the kinetic energy of the photoelectrons with a significantly lower falloff rate from one order to the next is expected for a tunneling/elastic-rescattering model. Beyond a kinetic energy of $10U_p$, the number of counts per ATI order will once again decrease quickly. The degree of the gentler falloff rate in the plateau region can vary dramatically from one element to another. For some elements, such as argon [4], the number of counts per order actually increases by almost an order of magnitude for kinetic energies within the plateau. Other elements such as helium [14,15], neon [14], and xenon [5] tend to have generally flatter plateau regions.

Although at first glance it appears that PES for magnesium completely lack a plateau region, it may be possible for two separate cases. First, the falloff rate from order to order in the plateau may be much closer to the initial falloff region, and consequently indistinguishable from characteristic (3). Second, the plateau photoelectrons may be physically present but with a very low probability, such that they reside below the noise floor. Between the two possible cases, the latter is less likely as longer data runs of up to 20×10^6 laser shots have been conducted, where the signal-to-noise ratio is

high for intensities below 60 TW/cm^2, and no significant plateau region has been observed. The seemingly complete lack of a PES plateau region is further discussed in Ref. [12], where Gillen *et al.* demonstrated that, based on ionization rate ellipticity studies, rescattering does not appear to be as dominant an ionization mechanism for magnesium as it is for the noble gases.

Experimental observation of a predicted PES cutoff is not as straightforward as it might first appear. If the signal-to-noise ratio is not high enough, the higher-kinetic-energy electrons can physically be present but lie beneath the floor of the noise and 1 not be detected. If the signal-to-noise ratio is high enough, or the decreasing rate of probability between the lowest and highest kinetic energy is low enough, electrons with kinetic energies up to and beyond the predicted cutoff can be detected. Due to the spread in initial conditions, a sharp classically predicted cutoff does not exist, but rather a more gradual and broad cutoff in the probability or signal exists. Thus, identifying a precise cutoff on a PES can be slightly subjective.

For the PES in Fig. 1 the ponderomotive potential is 2 eV, and the PES begins to fade into the noise around 13–16 eV. Thus, a soft cutoff threshold can be said to occur around $(6-7)U_p$. A cutoff energy of this value illustrates that high-intensity photoionization of magnesium is not easily categorized as either multiphoton or tunneling/rescattering.

B. Resonance structure within the first and second ATI order

When atoms are exposed to high-intensity laser light in the 1–100 TW/cm^2 intensity range, weakly bound, closely spaced energy levels have an ac Stark shift that is equal to the ponderomotive energy. As the intensity of the laser field increases, the intensity-dependent energy of these states increases. When the energy of a level equals that of an integer multiple of the photon energy, a Freeman resonance occurs and population shifts from the ground state of the atom to the resonant excited state, where it quickly ionizes by absorbing additional photons. Throughout this intensity range, ionization from excited states is clearly evident as a significant, if not a dominant, mechanism for magnesium. Photoelectron data obtained in these investigations illustrate that population of excited states via Freeman resonances and subsequent ionization is a very strong mechanism in the response of magnesium atoms to high-intensity laser light.

Figure 2 is a graph of numerous low-kinetic-energy intensity scans of PES collected for magnesium from 3 to 33 TW/cm^2. Note that even on a logarithmic scale, the height and width of the resonance peaks indicates that a significant number of the photoionized electrons are originating from atomic states other than the ground state. For the lower intensities the ATI peaks are structureless and appear to shift slightly to lower energies as the intensity increases to where the maximum signal of the MPI order is about 2000 counts. Below this intensity, each ATI peak is composed of unresolved high-lying Rydberg states which are ponderomotively shifted into resonance with a five-photon transition from the ground state. The apparent shifting of the structureless peak to lower kinetic energies is actually due to more unresolved

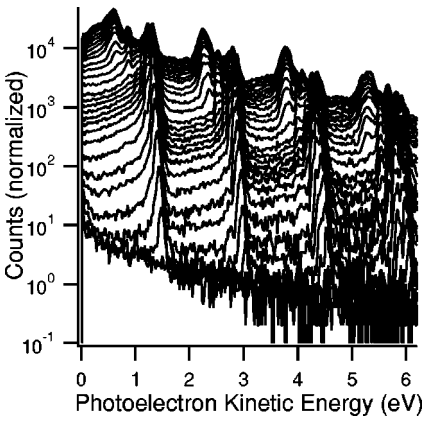

FIG. 2. Numerous PES of the MPI order and first three ATI orders for intensities ranging from 3 to 33 TW/cm^2.

Rydberg states coming into resonance as the five-photon resonant energy (5-PRE) probes deeper and deeper into the tightly spaced Rydberg states. These states appear on the low-kinetic-energy side of the ATI order and continue to grow in size and number as the intensity is increased, resulting in the illusion of a shifting, structureless ATI peak.

Further qualitative inspection of Fig. 2 reveals that as the intensity increases, and the 5-PRE probes deeper into the bound states, more resolvable excited atomic states become populated and subsequently ionized in the laser field leaving their signatures on the PES in the form of resolved peaks with different kinetic energies.

The next course of action is to identify specific states being populated utilizing angular momentum selection rules. Since the Freeman resonances occur for a five-photon transition from the ground state, we generally expect the states being populated to have an odd parity, limiting the possibilities to *p*, *f*, or *h* states. The kinetic energy of ionized electrons is $K=[m\hbar\omega-E_b]$, where E_b is magnitude of the binding energy of the chosen state, and m is the number of photons absorbed. Therefore, the kinetic energy of the freed electron is representative of the binding energy of the intermediate excited state at the time of ionization. If we assume that a collection of states all ac Stark shift by the same factor, then the relative spacing between adjacent peaks in the kinetic-energy spectrum corresponds to the relative spacing between adjacent states in the intensity-dependent energy-evel structure of the atom.

The series whose expected kinetic energies best match with the observed states are those of the *p* and *f* series. Within the energy resolution width of 0.015 eV (limited by the bandwidth of the laser) the *p* and *f* series energies are indistinguishable from each other. The energies of the *f* series and the measured PES for the first two ATI orders are illustrated in Fig. 3.

For intensities below 10 TW/cm^2 ($U_p=0.6$ eV), both ATI orders have similar peaks originating from 6 *f* and higher resonantly populated states, exhibiting threshold and growth characteristics expected from weakly bound, ponderomotively shifted states. For intensities above 10 TW/cm^2, peculiarities arise in the spectra, which are not easily explained using the basic ATI model. The first ATI

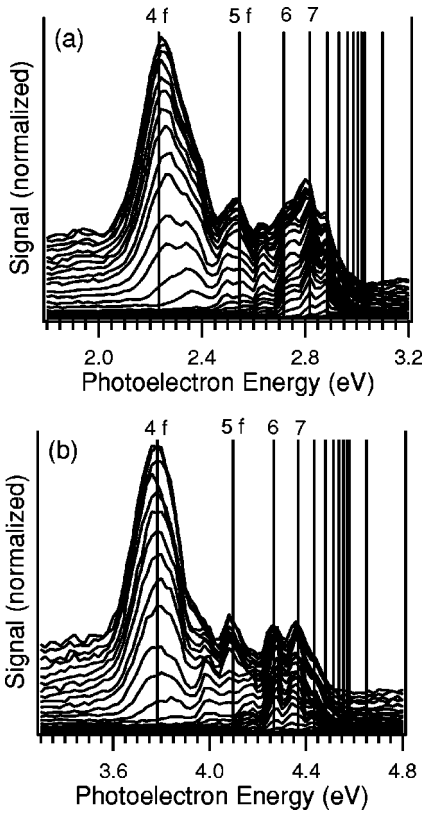

FIG. 3. Photoelectron spectra of the (a) first and (b) second ATI orders of magnesium atoms exposed to light intensities up to 33 TW/cm^2. The vertical lines correspond to theoretical kinetic energies of electrons ejected from *f*-series states ponderomotively shifted into a five-photon resonant transition from the ground state.

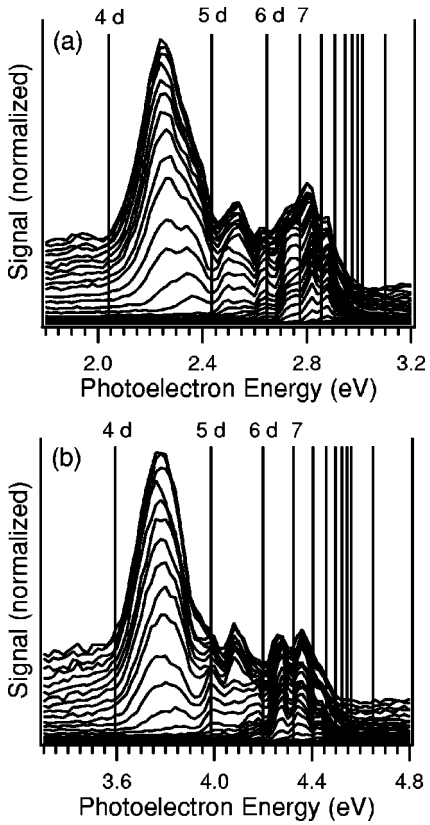

FIG. 4. Photoelectron spectra of the (a) first and (b) second ATI orders of magnesium atoms exposed to light intensities up to 33 TW/cm^2. The vertical lines correspond to theoretical kinetic energies of electrons ejected from *d*-series states ponderomotively shifted into a five-photon resonant transition from the ground state.

order contains peaks that have appearance intensities as expected for ponderomotively shifted states. Even so, there are many unexpected characteristics. First, a peak appears with an energy of 2.64 eV that does not correspond to a p or f state. A corresponding state appears in the second ATI order with an energy of 4.18 eV. For the first ATI order the peak remains there for all higher intensities. In the second ATI order, the shoulder of another peak for intensities above 19 TW/cm^2 over-runs the peak at 4.18 eV. This anomalous peak has the same energy expected of a ponderomotively shifted d state as illustrated in Fig. 4. The fact remains, however, that there should be no even number photon resonance populating a $6d$ state.

The very broad peak with energy from 2.1 to 2.4 eV in the first ATI order, and from 3.65 to 3.9 eV in the second ATI order, appears to be composed of two closely spaced, broad peaks. The higher-energy side of this structure appears around 14–15 TW/cm^2, with kinetic energies of 2.34 and 3.84 eV, while the lower-energy side appears around 17 TW/cm^2. In the first ATI order these two peaks are resolvable in the intensity range of 17–20 TW/cm^2. The lower-energy side of this structure overlaps with the expected kinetic energies of photoelectrons originating from a $4p$ or $4f$ state, while the higher-kinetic-energy side does not correspond to any ponderomotively shifted state.

In addition to the peculiar PES results mentioned above, the second-order ATI spectrum has additional unexpected results. A peak appears with a kinetic energy of 3.98 eV and does not have a counterpart in the first ATI order. This peak is seen in Figs. 3 and 4, and coincidentally overlapped with the $5d$ energy line. A counterpart in the first ATI order would have an energy of 2.43 eV, where there is actually a minimum in the PES. The appearance of a feature in one ATI order and not in another is not explained by the basic ATI model. Thus the possibility that this energy peak originates from a resonantly populated bound state that subsequently ionizes via a higher-order process, but not a lower-order process, is very unlikely.

The preceding analysis is based solely on multiphoton resonances with Rydberg states of the neutral atom. As with all alkaline-earth-metal atoms, many low-lying states of the magnesium ion are easily accessible at these intensities. Estimates of the ac Stark shift using second-order perturbation theory show that the $3p$ levels of the ion shift by about $0.1U_p$. Since perturbation theory is of dubious value at these intensities, these estimates are only rough guides. The highest intensities in this study are about 30 TW/cm^2, giving $U_p = 1.8$ eV and maximum Stark shifts of about 180 meV. Thus, the $3p$ levels undergo a total shift of about $1.1U_p$ or an additional 180 meV beyond the ponderomotive shift for the first electron relative to the neutral ground state. Any au-

toionizing Rydberg states converging on the $3p$ levels may participate in eight photon resonances and could, therefore, appear in the PES at the locations of *d* states amongst the odd-parity *p* or *f* states. As will be discussed in Sec. III C, the appearance intensities of these anomalous features correspond to states converging on the first ionization limit and not excited ionic levels.

C. Partial yields and angular distributions

In Sec. III B we observed that numerous excited states were populated and subsequently ionized by the applied laser field. As the laser intensity increased, deeply bound states tuned into a five-photon resonant transition from the ground state. A first-pass analysis of the data, based upon angular-momentum selection rules, indicates that the states being populated are of an odd parity, and most likely *p* or *f* states. By simply matching up the expected kinetic energies observed with those expected for either a *p* or *f* state, it could not be determined whether the electrons originated from a Freeman resonance to a *p* or an *f* state due to the overlap of the energies of these two series. In this section we present two methods for (1) better identification the threshold necessary to initiate the Freeman resonance, and (2) better identification of the parity and angular momentum of the state from which the electron ionized.

A PY is a data analysis method where only a small range of the photoelectron kinetic energies is integrated within a single PES. The integration is then repeated for a variety of peak laser intensities, and the resulting PY is displayed as the number of integrated counts per PES as a function of the peak laser intensity. By observing the change in counts as a function of peak laser intensity, the threshold intensity for a given resonant process can be more quantitatively identified than by simple inspection of multiple PES displayed on the same graph. An expected PY curve for a single-ionization channel, using a restricted laser-atom interaction volume, has similar characteristics as those expected for restricted volume ionization yield experiments. The yield does not grow appreciably until the threshold intensity is reached. Once the threshold intensity is reached, the rate of ionization through that channel increases rapidly until saturation where the rate of increase of signal levels out, as the restricted Gaussian volume does not continue to grow for increasing peak intensities. The ionization volume, for a particular process, adopts the shape of an annulus whose inner and outer radii increase with increasing intensity such that the total volume remains constant.

AD plots have been used for many years to aid in the interpretation of PES collected for strong-field ionization of atoms. Much of the interpretation of the results has been the identification of high probability scattering angles, or ''jets,'' as the ionized electron scatters off of the core during its motion in the laser field [5,16,17]. It has been observed that as the laser field drives the electron, it has the highest probability to scatter off of the core at angles of 30° and 45°. The observation of the scattering angles for selected regions of the kinetic energies of ejected electrons was yet another supporting argument that the plateau extension observed in the photoelectron spectra for the noble gases is a result of a rescattering mechanism. The scattering jets for xenon are most pronounced for electrons with energies of $(8-10)U_p$ [5,17]. The earlier investigations were unable to resolve the structure within each ATI order, which results in an AD that is averaged over an entire ATI order, while a later investigation by Nandor *et al.* [5] illustrated that within each order the appearance of the ADs can vary quite remarkably.

Although AD plots have been used to identify rescattering mechanisms, they have also been used to help identify the angular momenta carried away by the electron as it is ionized, and the parity of its last state, for lower ATI orders [5,18,19].

The fact that the observed angular distributions can both be a measure of the angular momentum of the last state of the electron and the angular scattering probability of a free electron scattering off of its parent ion, reduces the absolute validity of claiming either one. Nevertheless, considering which ionization processes are dominant and what region of kinetic energies is being studied, the uncertainty of interpreting ADs can reduced. If the dominant ionization process is multiphoton in nature, then the angular momentum carried away by the electron will also be multiphoton in nature. For this case, the ADs will more likely be a reflection of the angular momentum of the last state of the electron. Since higher-energy electrons are produced predominantly by a rescattering mechanism, the angular distributions for higher kinetic energies will reflect the angular scattering probability. This assumption holds especially true for photoelectrons whose kinetic energies fall with the plateau region [5,16,17].

For low-kinetic-energy electrons and multiphoton processes, ADs can reveal properties of the last state of the electron. As an example, consider an electron that is excited through a $5f$ state of the atom. The electron absorbs one more photon to get to the MPI order, exciting it into an unbound *d* or *g* state carrying away an angular momentum of $l=2$ or 4. Thus, for this simplistic case, we would expect the AD to reflect a superposition of *d* and *g* angular probability distributions.

Figure 5 is a collection of PES, PYs, and ADs for the high-lying Rydberg states with kinetic energies above 2.7 eV and 4.2 eV in the first and second ATI orders, respectively. It is organized into two columns with the left column, displaying data for the first ATI order and the right column displaying data for the corresponding energy range in the second ATI order. The energy range of interest is displayed in the top PES graph, Figs. 5(a) and 5(b). A few intensities are displayed in each PES to illustrate the general trend of the electron energy dependence on the peak laser intensity. Figures 5(c)–(f) are PY plots of the integration over the energy range as a function of peak laser intensity. The two vertical lines in the PY represent the threshold intensities for the ponderomotively shifted 5-PRE to drop to a level whose binding energy would result in ionized photoelectrons with kinetic energies that correspond to the maximum and minimum energies of the energy range of interest. Figures 5(g)–(j) are the AD data for the chosen energy ranges. The angular distributions are collected for a peak field intensity of 23 TW/cm^2. Each point on the AD is an integration of the

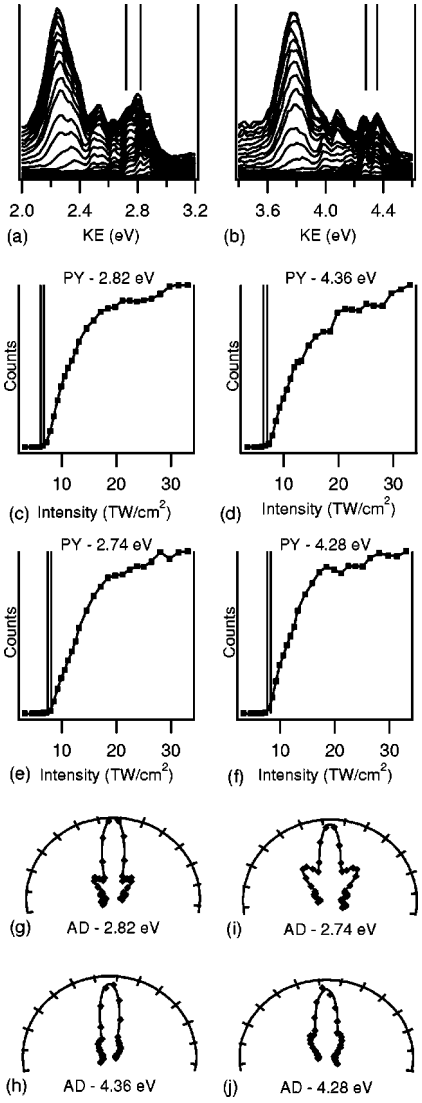

FIG. 5. Photoelectron spectra of the (a) first and (b) second ATI orders. The vertical lines in (a) and (b) represent the kinetic-energy peaks that correspond to resonantly populated $6f$ and $7f$ states. (c)–(f) are partial-yield plots, and (g)–(j) are angular distribution plots for those peaks. The energy width integrated for the PY and AD plots is 0.02 eV. The vertical lines in the PY plots represent the theoretical threshold intensities necessary to resonantly populate a state that would result in an electron with the upper and lower range of kinetic energies integrated.

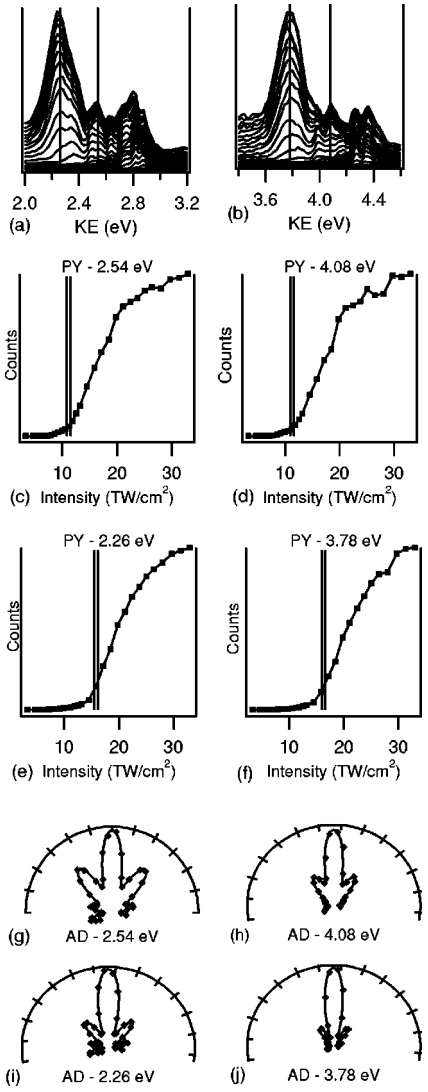

FIG. 6. Photoelectron spectra [(a) and (b)], partial-yield plots [(c)–(f)], and angular distribution plots (g)–(j), for photoelectron peaks corresponding to resonantly populated $4f$ and $5f$ states.

chosen range of kinetic energies, for a particular orientation of the laser field with respect to the flight path. Since the parity of the final state of the electron is expected to be either even or odd, the AD data are normally fit with a sum of either even or odd Legendre polynomials. The fits of the Legendre polynomials serve a dual purpose. First, the fits allow for a smooth representation of the AD data, and second the coefficients of the fits can aid in the identification of the angular momenta of the possible final states.

For all energy ranges analyzed in Fig. 5, an inspection of the PYs reveals that the increase in the integrated number of counts as a function of peak intensity correlates well with the expected threshold for ponderomotively shifted states. The number of counts for the chosen energy ranges does not significantly increase until the threshold intensity is reached in order to ponderomotively shift the state into a five-photon Freeman resonance. The ADs for the first order illustrate three distinct lobes per quadrant. The highest count rate is observed for the orientation of $0°$, or parallel to the flight path, and two more maxima located at $36°$ and $70°$. At an angle of $90°$ a minimum is observed, as would be expected for a superposition of various odd states. Although a minimum is observed for a $90°$ orientation between the laser field and the flight path, the count rate still does not go to zero. The best fit of the data (mainly to correct for a nonzero count rate for $\pm 90°$) was found to be the one that included a 10% contribution from even Legendre polynomials. This value takes into account the possibility of producing ionization through an even number of photons either through excited ion states or via double ionization.

The PYs and ADs for the other two observed f states, the $4f$ and the $5f$, are displayed in Figure 6. The observed

TABLE I. Summary of the states populated via a five-photon Freeman resonance from the ground state, the resonant threshold intensity, and observed kinetic energies (KE) for the first and second ATI orders.

State	Threshold intensity (TW/cm^2)	KE First ATI (eV)	KE Second ATI (eV)
$8f$	5.4	2.88	4.42
$7f$	6.5	2.82	4.36
$6f$	8.1	2.73	4.27
$5f$	11.0	2.54	4.09
$4f$	16.3	2.24	3.78

threshold intensities for ionization through the $4f$ and $5f$ states do not exhibit a turn-on as sharp as that observed for the higher f states, but still agree with the calculated threshold for ponderomotively shifting states. Table I summarizes the resonant state, threshold intensity, and kinetic energy for above threshold ionization from that state, for all of the states studied in Figs. 5 and 6.

Ion yield measurements discussed in Ref. [12] indicate that for the peak field intensity used to collect the ADs, 23 TW/cm^2, roughly 10–20 % of the ions detected are doubly charged ions. If a singly charged ion is present in the interaction region its energy levels will be ponderomotively shifted through an even parity state and subsequently ionize. If the ion is originally in its ground state and encounters a ten-photon Freeman resonance, it will ionize from an even-parity state. A calculation performed by Xenakis *et al.* [20] for magnesium atoms exposed to similar laser pulses using 400 nm predicted that photoionization from $Mg(3s)^2$ to Mg^+3p is a non-negligible process. Even if a significant fraction of the Mg^+ ions are created in the first excited state, they will encounter a seven-photon Freeman resonance from an odd-parity state to an even-parity state and subsequently ionize. Thus, a mixture 10% odd and even coefficients of Legendre polynomial coefficients for the fits to the AD data is justifiable, and an accurate representation of the different ionic species is produced.

For all of the numerical fits to the observed data, the largest coefficients indicate that the most significant angular-momentum contributions have values of $l=1$, 3, and 5 for the first ATI order, and $l=0$, 2, 4, and 6 for the second ATI order. Table II is a summary of the odd Legendre polynomial coefficients used for the fits of the angular distributions for the first ATI order peaks analyzed in Figs. 5 and 6. Both observed number of AD lobes and the results of fits using Legendre polynomials indicate that the dominant initial states populated via a Freeman resonance must be those of f states.

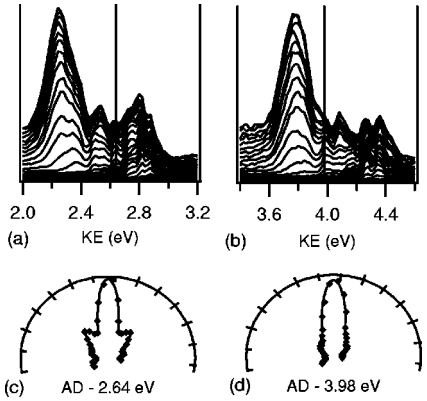

FIG. 7. Photoelectron spectra and angular distributions for two peaks that do not have a clear counterpart in the other ATI order. The angular distributions exhibit a fundamentally different structure than that which is observed for other nearby peaks.

As mentioned in Sec. III B, in addition to the expected Freeman resonance transitions from the ground state to odd-parity states, the PES reveal some unexpected results. Each ATI order possesses characteristics that do not appear to have equal counterparts in the other ATI order.

Unlike Figs. 5 and 6, which highlight the similarities between the first and second ATI orders, Fig. 7 investigates some of their differences. The energy ranges and ADs for two of the order-to-order variations observed are displayed in Fig. 7. The first ATI order contains a peak with a kinetic energy of 2.64 eV with distinct minima on either side of it located at 2.60 and 2.68 eV, as illustrated in Fig. 7(a). A counterpart in the second ATI order would have a kinetic energy of 4.19 eV. Although there is a slight peak at this expected energy for lower intensities, the PES is much more uniform between 4.05 and 4.2 eV for intermediate and higher intensities. The minima on either side of the peak at 4.19 eV, especially on the lower-kinetic-energy side, are much less pronounced than they are for the corresponding peak in the first ATI order. The angular distributions for these energies

TABLE II. Summary of the odd Legendre polynomial coefficients used in the fits for the first ATI order peaks discussed in Figs. 5 and 6. For easier comparison, all coefficients for each fit are normalized such that the sum of their squares is 1.

State	$l=1$ coefficient	$l=3$ coefficient	$l=5$ coefficient	$l=7$ coefficient	$l=9$ coefficient	$l=11$ coefficient
$8f$	0.63	0.38	0.56	0.18	0.27	0.19
$7f$	0.61	0.11	0.77	0.01	0.08	0.04
$6f$	0.56	0.10	0.78	0.18	0.02	0.19
$5f$	0.27	0.13	0.89	0.29	0.14	0.08
$4f$	0.26	0.64	0.42	0.57	0.09	0.12

do not significantly differ from those for the rest of the peaks with nearby kinetic energies. Overall, the PES for each ATI order possess different characteristics for these corresponding energy ranges; with the first ATI order possessing more clearly resolved structure between the $5f$ and $6f$ kinetic energies.

The peak that appears in the second ATI order with a kinetic energy of 3.98 eV is altogether unique, and highlighted in Fig. 7(b). As discussed in Sec. III B, this peak appears only in the second ATI order and a corresponding energy in the first ATI, 2.44 eV, is actually the position of a minimum in the PES. Similar to the other peaks discussed, the location of the peak in the PES does not correspond to a ponderomotively shifted bound state. But, unlike the other anomalous peaks discussed, the angular distribution of ejected electrons measured for this peak, Fig. 7(d), do differ significantly from the rest of the peaks observed in that kinetic-energy range and within the second ATI order. The angular ejection of electrons from the interaction region with this kinetic energy poss a noticeably different visual appearance with the near absence of minor lobes or ''jets,'' and the coefficients required to fit this angular distribution are generally different than those used for the rest of the peaks within the second ATI order. A more even mixture of even and odd Legendre polynomials was required to simulate the single uniform lobe appearance.

Both peaks observed in Fig. 7 do not correspond to any expected Freeman resonance transitions from the ground state to odd-parity ponderomotively shifted states, and illustrated in Fig. 3. One explanation for the observation of photoelectron kinetic energies that do not correspond to resonant population and subsequent ionization of ponderomotively shifted states is simply that the shift of the intermediate state is nonponderomotive. The binding energy of a nonponderomotively shifted state is intensity dependent, resulting in a photoelectron kinetic energy that can vary depending upon the instantaneous laser intensity of both the resonant transition and the moment of subsequent ionization. Since the shift of nonponderomotively shifted states is unknown, the resulting photoelectron kinetic energy is also unpredictable. Without additional knowledge of the original state or a verifiable prediction of its ac Stark shift claiming a particular peak as originating from a nonponderomotive source cannot be made with any degree of certainty. Therefore the origin of the unidentifiable peaks discussed is still largely unknown at this point.

It should be noted here that the second ATI order has one property that is present for no other ATI order. One possible reason why a photoelectron can have a kinetic energy in the range of 3–4 eV, and no other value for integer photon energies above or below this range, is that it originated from a doubly excited autoionizing state. The energy limit for any $3pNl$ doubly excited state is the $Mg^+(3p)$ level, or 4.422 eV above $Mg^+(3s)$. Historically, the $3pNs$ and the $3pNd$ doubly excited states are well known due to the experimental availability of these states [21–24]. Although the energies of these known states do not overlap well with the anomalous peaks of 3.98, 4.08, and 4.18 eV, the possibility that these order-specific peaks originate from unmapped autoionizing states cannot be ruled out completely.

IV. CONCLUSIONS

We have collected photoelectron spectra for magnesium atoms exposed to 800-nm, 120-fs laser pulses with peak intensities from 3.3×10^{12} to 4.0×10^{13} W/cm^2. Throughout the entire intensity range, the magnesium PES do not reveal a significant production of hot electrons or a rescattering plateau region, which is not at odds with the results of ion yield measurements where it is demonstrated that enhanced double ionization is multiphoton in nature and not rescattering. The absence of this characteristic demonstrates that much of the ionization process for magnesium differs from that which is calculated and observed for noble gases. Although a significant plateau extension out to $10U_p$ is not detected for magnesium, observed cut off kinetic energies are in the $(6-7)U_p$ range for linearly polarized light, and $(4-5)U_p$ range for circularly polarized light. Thus, rescattering cannot be ruled out completely as a contributing ionization mechanism for the higher range of observed photoelectron kinetic energies. The plateau observed for intensities higher than 2×10^{14} W/cm^2 is attributed to the photoionization of the Mg^+ ion.

For intensities up to 10 TW/cm^2, the PES consists of expected high-lying, odd-parity, Rydberg states ponderomotively shifted into a five-photon Freeman resonance. Kinetic-energy studies indicate that the excited states populated are p or f states. Further analysis using angular distributions indicate that the intermediate excited states are mostly composed of f states. PES collected for intensities in the region of 10–40 TW/cm^2 exhibit some unexpected structures in the PES. Photoelectron peaks appear in both the first and second ATI orders with energies that do not correspond to five-photon resonant transitions from the ground state to odd-parity excited states.

In addition, we have also observed different structures from one ATI order to another. Order-specific structures of the second ATI occur in an energy range that contains numerous doubly excited autoionizing states, both well known and unmapped. The angular distribution data for the kinetic-energy peak of 3.98 eV is fundamentally different from the angular distributions observed for most of the other peaks within the second ATI order.

The explanation for the observation of these characteristics is not known at this point, and current ATI models cannot explain how these order-to-order variations can occur. The fact that these anomalies are observed and not easily explained indicates that photoionization experiments in magnesium offer new perspectives on strong-field ionization, which complement the work on noble gases.

ACKNOWLEDGMENTS

The authors would like to thank P. Randerson for help with this paper. This work was supported by the NSF under Grant No. 9876965.

[1] G.S. Voronov, and N.B. Delone, Sov. Phys. JETP **1**, 66 (1965).
[2] P. Agostini *et al.*, Phys. Rev. Lett. **42**, 1127 (1979).
[3] R.R. Freeman *et al.*, Phys. Rev. Lett. **59**, 1092 (1987).
[4] M.J. Nandor, M.A. Walker, and L.D. Van Woerkom, and H.G. Muller, Phys. Rev. A **60**, R1771 (1999).
[5] M.J. Nandor, M.A. Walker, and L.D. Van Woerkom, J. Phys. B **31**, 4617 (1998).
[6] M.A. Walker, P. Hansch, and L.D. Van Woerkom, Phys. Rev. A **57**, R701 (1998).
[7] P. Hansch, M.A. Walker, and L.D. Van Woerkom, Phys. Rev. A **55**, R2535 (1997).
[8] P. Hansch, M.A. Walker, and L.D. Van Woerkom, Phys. Rev. A **57**, R709 (1998).
[9] P. Hansch, and L.D. Van Woerkom, Opt. Lett. **21**, 1286 (1996).
[10] H. Rottke *et al.*, Phys. Rev. A **49**, 4837 (1994).
[11] H. Rottke, J. Ludwig, and W. Sandner, Phys. Rev. A **54**, 2224 (1996).
[12] G.D. Gillen, M.A. Walker, and L.D. Van Woerkom, Phys. Rev. A **64**, 043413 (2001).
[13] A. Lohr, M. Kleber, R. Kopold, and W. Becker, Phys. Rev. A **55**, R4003 (1997).
[14] B. Sheehy *et al.*, Phys. Rev. A **58**, 3942 (1998).
[15] B. Walker *et al.*, Phys. Rev. Lett. **73**, 1227 (1994).
[16] B.C. Walker, *One-and Two-Electron Ionization of Atoms by a Strong Laser Field* (State University of New York, Stony Brook, 1996).
[17] B. Yang *et al.*, Phys. Rev. Lett. **71**, 3770 (1993).
[18] Y. Gontier, and M. Trahin, JOSA B **7**, 463 (1990).
[19] H. Rottke *et al.*, Z. Phys. D: At., Mol. Clusters **15**, 133 (1990).
[20] D. Xenakis *et al.*, Phys. Rev. A **60**, 3916 (1999).
[21] G.W. Schinn, C.J. Dai, and T.F. Gallagher, Phys. Rev. A **43**, 2316 (1991).
[22] C.J. Dai, G.W. Schinn, and T.F. Gallagher, Phys. Rev. A **42**, 223 (1990).
[23] H.C. Chi, and K.-N. Huang, Phys. Rev. A **50**, 392 (1994).
[24] R. Moccia, and P. Spizzo, J. Phys. B **21**, 1121 (1988).